

Evolutionary Kuramoto dynamics unravels origins of chimera states in neural populations

Thomas Zdyski¹, Scott Pauls¹, and Feng Fu^{1,2}

¹Department of Mathematics, Dartmouth College, Hanover, NH 03755

²Department of Biomedical Data Science, Geisel School of Medicine at Dartmouth, Lebanon, NH 03756 .

Abstract

Neural synchronization is central to cognition^{1,2}. However, incomplete synchronization often produces chimera states^{3,4}, where coherent and incoherent dynamics coexist. While previous studies⁵ have explored such patterns using networks of coupled oscillators, it remains unclear why neurons commit to communication or how chimera states persist. Here, we investigate the coevolution of neuronal phases and communication strategies on directed, weighted networks, where interaction payoffs depend on phase alignment⁶ and may be asymmetric due to unilateral communication. We find that both connection weights and directionality influence the stability of communicative strategies—and, consequently, full synchronization—as well as the strategic nature of neuronal interactions. Applying our framework to the *C. elegans* connectome^{7–9}, we show that emergent payoff structures, such as the snowdrift game, underpin the formation of chimera states. Our computational results demonstrate a promising neurogame-theoretic perspective, leveraging evolutionary graph theory to shed light on mechanisms of neuronal coordination beyond classical synchronization models.

1 Introduction

Evolutionary game theory (EGT) is the application of game theory to evolving populations of individuals with behavioral strategies. This tool is useful for studying how local interaction rules yield large-scale patterns such as cooperation¹⁰ and has found use in fields including international politics, ecology, and protein

folding¹¹. Studies^{6,12,13} have even applied EGT to non-reproducing neurons by viewing neuron plasticity as an evolutionary process where firing patterns change and are “learned” over time. Evolutionary graph theory places evolutionary games on graphs to investigate the role of structure in population evolution. Prior studies have found that structure qualitatively changes

game evolution. For instance, cooperation is enhanced by small-degree nodes¹⁴ or unidirectional edges¹⁵ and suppressed by weighted edges¹⁶. Thus, the study of evolving, structured populations should account for the effects of incompleteness, directedness, and weightedness.

Kuramoto networks are groups of coupled oscillators where the coupling strength depends sinusoidally on the oscillators' phase difference. These networks are popular models for neuron behaviour^{17,18} because they exhibit tunable synchronization. Prior studies¹³ have modelled interneuron communication with Kuramoto oscillators and EGT using the prisoner's dilemma game type. Other studies⁶ generalized this approach to include dynamically changing game types by introducing an evolutionary Kuramoto (EK) model to show how the relationship between communication benefit and cost influences the emergence of synchronized communication or non-communication regimes.

One intriguing aspect of neuron oscillations is the observation of chimera states³. These states exhibit the simultaneous existence of coherent and disordered phases⁵. Previous studies have proposed chimera states as a key component of human cognitive organization², a facilitator of spiking and bursting phases¹, and an outcome of modular networks⁴. Despite the observed importance of these chimera states, the factors that give rise to coherent/disordered coexistence remain incompletely characterized.

The nematode *Caenorhabditis elegans* (*C. elegans*) is a model organism in neuroscience due to its simple brain connectome⁷ of only 302 neurons. Despite their simplicity, models of the *C. elegans* brain still display a wide array of complex phenomena including topologically-central

rich clubs crucial to motor neurons⁸, phenomenological connections to control theory⁹, and chimera states⁴.

In this paper, we introduce an asymmetric evolutionary Kuramoto model and analyze its chimera-like states on the *C. elegans* connectome. Our results connect individual neuron fitness and non-trivial brain topology to chimera-like brain states. Given current technological limitations with direct measurement of in-vivo neuron activity, frameworks like ours create testable hypotheses connected to the theory's assumptions. Our computational model represents a simple yet versatile framework to illuminate the influence of neural connectivity on chimera-like brain states beyond classical synchronization models.

2 Results

2.1 Model

We extend the EK model in two ways: placing the player network on a directed, weighted graph; and introducing a payoff asymmetry. First, we represent a well-mixed population as a complete graph in Fig. 1(a) with players represented by nodes and games by edges. We generalize this to directed graphs where game (edge) payoffs only flow to the head players (nodes). We can also represent bidirectional games with a pair of edges in both directions, as shown in Fig. 1(b). For reference, the *C. elegans* connectome has 38 self-loops, 669 bidirectional edge pairs, and 2,331 unpaired edges. Finally, we interpret the *C. elegans* chemical connectome's integer-valued edge weights as the number of connections between nodes, so these weights scale each payoff.

We also generalize the payoff structure to incorporate an asymmetry between communicators and non-communicators.

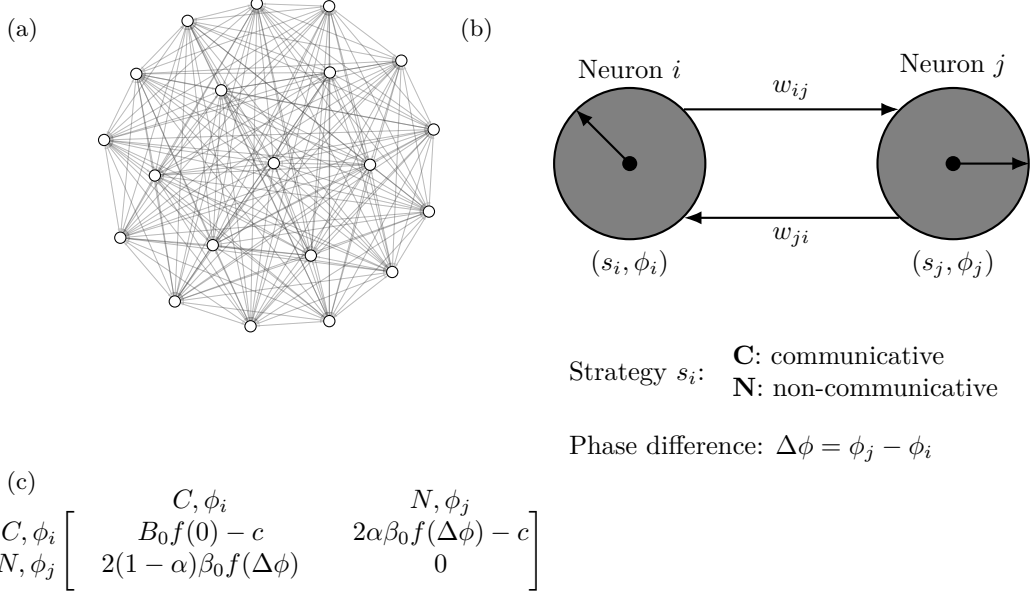


Fig. 1| Evolutionary Kuramoto dynamics with weighted neural connectivity.

(a) The graph of a well-mixed population with $N = 20$ players where each pair of players is connected by a directed edge in each direction. (b) The connectivity between two sample players, i and j , showing directed, weighted edges w_{ij} and w_{ji} . Each player has a strategy (communicative C or non-communicative N) and phase $\phi = 2\pi k/m$ with $k \in 0, \dots, m-1$ and m the number of phases. (c) The payoff matrix shows the reward the row-player (C, ϕ_i) receives after playing a game with the column-player (N, ϕ_j) assuming either player can switch strategy and phase to the other's.

We characterized each player (node) by its strategy s_i —either communicative C or non-communicative N —and its phase ϕ_i —taking one of $m = 20$ evenly-spaced values between 0 and 2π . When exactly one partner is communicative, the asymmetry $\alpha \in [0, 1]$ biases the payoff toward (against) the communicator when α is greater (less) than $1/2$, while $\alpha = 0.5$ reproduces the symmetric case. Figure 1(c) shows the payoff matrix for these mixed CN or NC interactions and includes the maximum joint benefit $B_0 = 0.15$, maximum mixed benefit β_0 , cost c , and sinusoidal

Kuramoto coupling $f(\Delta\phi) = [1 + \cos(\phi_j - \phi_i)]/2$.

Unless otherwise specified, each simulation uses $m = 20$ phases, selection strength of $\delta = 0.2$, mutation rate of $\mu = 1 \times 10^{-4}$, cost c of 0.1, maximum joint benefit $B_0 = 0.15$, maximum mixed benefit β_0 of $0.95B_0$, and runs for 8×10^6 time steps (even if only a smaller time series subset is shown).

2.2 Parameter space

One of the key aspects of the EK model is that multiple 2×2 game

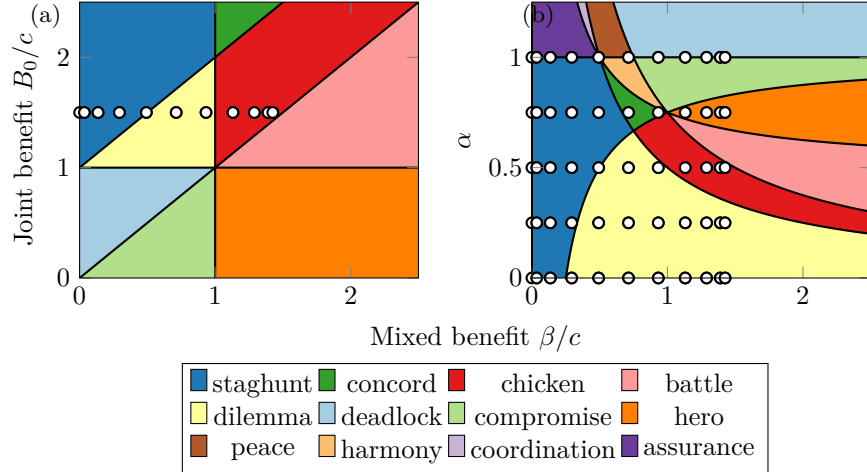


Fig. 2| Payoff asymmetry enriches neural interactions well beyond the classic prisoner’s dilemma game type. Region plots illustrate the diverse range of game types that neural populations can engage in during evolutionary dynamics. Slices of the three-parameter mixed CN game-type phase diagram in the (a) β - B_0 plane ($\alpha = 0.5$) and (b) β - α plane ($B_0/c = 1.5$). For two players with phase difference $\Delta\phi$, the mixed benefit is $\beta = \beta_0[1 + \cos(\Delta\phi)]/2$. The legend displays the game type corresponding to each color. The white dots represent the $m = 20$ potential phase differences as well as the restriction (a) $B_0/c = 1.5$ or (b) $\alpha \in [0, 0.25, 0.5, 0.75, 1]$.

types can emerge among the players during the population’s evolution. These game types¹⁹ include dilemma (*a.k.a.* “prisoner’s dilemma”), deadlock (“anti-prisoner’s dilemma”), chicken (“hawk-dove” or “snowdrift”), hero (“Bach or Stavinsky” with the lowest two payoffs swapped), harmony (game with strong incentive alignment), or concord (similar to harmony, weaker incentives). See Section 2 of the supplementary material for order graphs depicting the payoff structure of each game type. While CC interactions are always double-cooperation games and NN interactions are always neutral games, mixed (CN or NC) games show a variety of game types, (Fig. 2). We can visualize these games by looking at two-dimensional slices of the three-dimension phase space characterized by α ,

$\beta := \beta_0 f(\Delta\phi)$, and B_0 . Fig. 2(a) shows a β - B_0 slice of phase space and generalizes figure 1 of a prior study⁶, while Fig. 2(b) shows a β - α slice. Each straight line of white dots represent permissible values of the $m = 20$ phases $\Delta\phi_i$ across our simulations and highlight which regions of parameter space are accessible.

2.3 Complete graphs

First, we will explore the influence of the newly introduced asymmetry on a $N = 20$ -player, well-mixed population. Figure 3(a) compares the frequency of communicative strategies f_{comm} to the maximum joint benefit B_0 . The marks represent the simulation results and the lines represent the full analytic result (Eq. 10 in supplementary material) for a well-mixed population.

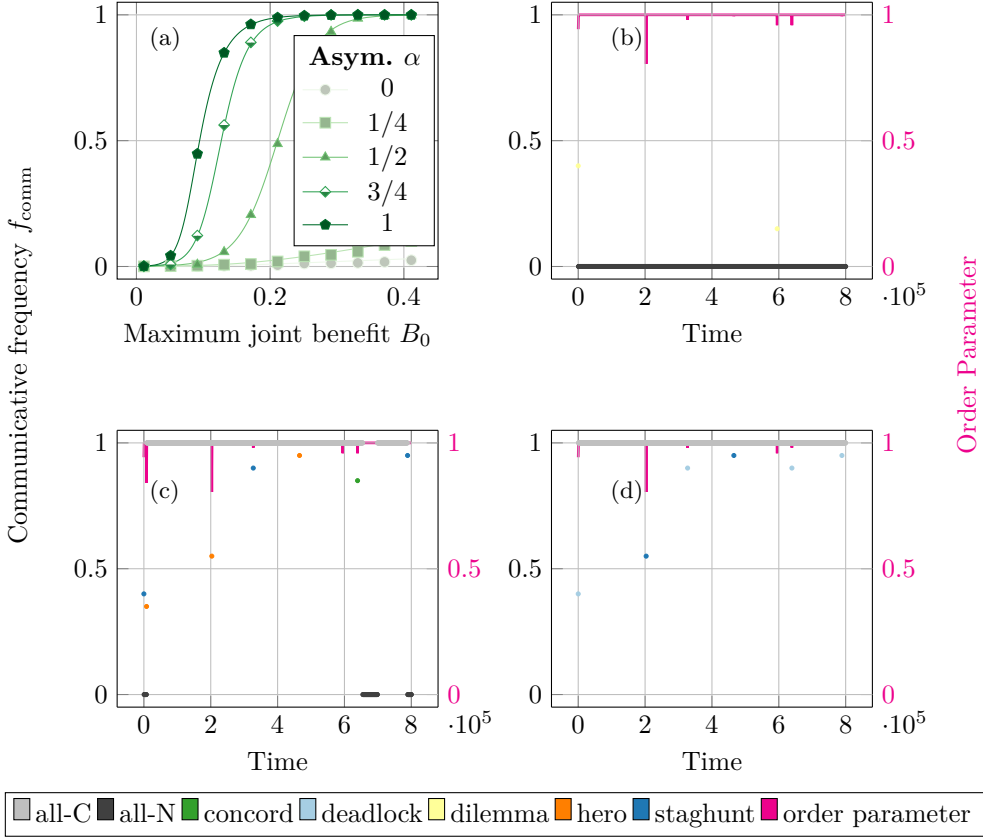


Fig. 3| Impact of symmetry breaking on neural synchronization in well-mixed populations. Communication frequency f_{comm} for the well-mixed topology. (a) Time-averaged f_{comm} as a function of the maximum joint benefit B_0 for different values of the payoff asymmetry α . The marks represent the simulation results and the lines represent the theory predictions. (b)–(d) Scatter plots where the left vertical axes show the instantaneous f_{comm} as a function of time and are color-coded according to the plurality mixed game type as indicated in the legend. The right vertical axes give the order parameter ρ (Eq. 4), in magenta, as a function of time. The asymmetry is (b) $\alpha = 0$, (c) $\alpha = 0.75$, and (d) $\alpha = 1$.

The B_0 step size is 0.04, and the simulations ran for 2×10^8 time steps. In general, f_{comm} is low for small B_0 , rises to $f_{\text{comm}} = 0.5$ at some break-even B_0 , and plateaus to $f_{\text{comm}} \approx 1$ for large B_0 . We can validate our model by comparing our $\alpha = 0.5$ case with a previous study⁶ to

observe qualitatively similar results, with our break-even $B_0 \approx 0.21$ corresponding to their $B_0 = 2(N-1)c/(N-2) = 0.21$ break-even condition. We also see that increasing (decreasing) the asymmetry α dilates (stretches) this sigmoid function in the B_0 direction. This α -dependence is

reasonable, as increasing α corresponds to biasing the payoff in a mixed *CN* interaction towards the communicative partner.

While Fig. 3(a) displays the time-averaged system state, it is also useful to investigate the time-dependent variations. Figures 3(b) to 3(d) depict the frequency of communicative strategies f_{comm} as scatter plots of time on the left vertical axis for different values of the asymmetry α . These time-series points are color-coded grey if all players are communicative or black if all players are non-communicative; otherwise, the points are colored according to the plurality mixed game type, as indicated in the legend. On the right vertical axes, magenta line plots depict the order parameter $\rho \in [0, 1]$ given by Eq. (4).

Figure 3(b) shows the time-variation when the system heavily favors non-communicative players with $\alpha = 0$. After an initial disordered, dilemma-type game (yellow), the system synchronizes in the non-communicative regime (black line at $f_{\text{comm}} = 0$) with only a brief dilemma-type game excursion near time step 6×10^5 . Figure 3(c) depicts an asymmetry $\alpha = 0.75$ that moderately encourages communicativeness. The system is synchronized in a communicative state (gray line at $f_{\text{comm}} = 1$) 92 % of the time, with unstable excursions to synchronized, non-communicative states (black line at $f_{\text{comm}} = 0$) and disordered, hero (orange) and staghunt (dark blue) game types. This 92 % communicative rate is higher than the expected 75 % from Fig. 3(a) (for $B_0 = 0.15$ and $\alpha = 0.75$), likely due to the small timespan shown in Fig. 3(c). Finally, Fig. 3(d) shows the $\alpha = 1$ case where communication is heavily incentivized. Like the (b) $\alpha = 0$ case, the system is virtually always synchronized in the communicative

regime, with only brief excursions to deadlock (light blue) or staghunt (dark blue) games types. We note that all three (b)-(d) scenarios are virtually always synchronized; the order parameter ρ (magenta) is almost always $\rho = 1$, with only occasional dips. The temporary drops in communicative frequency f_{comm} and order parameter ρ are likely the result of mutations which occur, on average, every $1/\mu = 1 \times 10^4$ time steps.

2.4 *C. elegans* graphs

Here, we consider the weighted, directed hermaphroditic *C. elegans* chemical connectome⁷. For reference, Fig. 4(d) shows the $N = 300$ nodes and the directed edges (we exclude the two unconnected neurons CANL/CANR). The nodes are colored according to their strategy at a particular time step, with blues representing communicative strategies and reds representing non-communicative ones, and different shades corresponding to different phases ϕ . We note the chimera-like character of the large, synchronized group of red nodes coexisting with disordered neighboring nodes.

Next, to quantify the observations of Fig. 4(d), Fig. 4(a) shows the fraction of players using communicative strategies f_{comm} averaged across the entire simulation of 2×10^8 time steps as a function of the maximum joint benefit B_0 in 0.04 steps for the *C. elegans* connectome network topologies. All subplots use an asymmetry of $\alpha = 0.75$.

We note that the behaviour of the (a) *C. elegans* case is qualitatively distinct from the $\alpha = 0.75$ well-mixed case in Fig. 3(a). The communicative fraction f_{comm} is flatter for $B_0 \leq 0.08$, has a steep jump to 0.77 at $B_0 = 1.6$, and decreases to a horizontal asymptote around 0.60. We can isolate the cause of this deviation

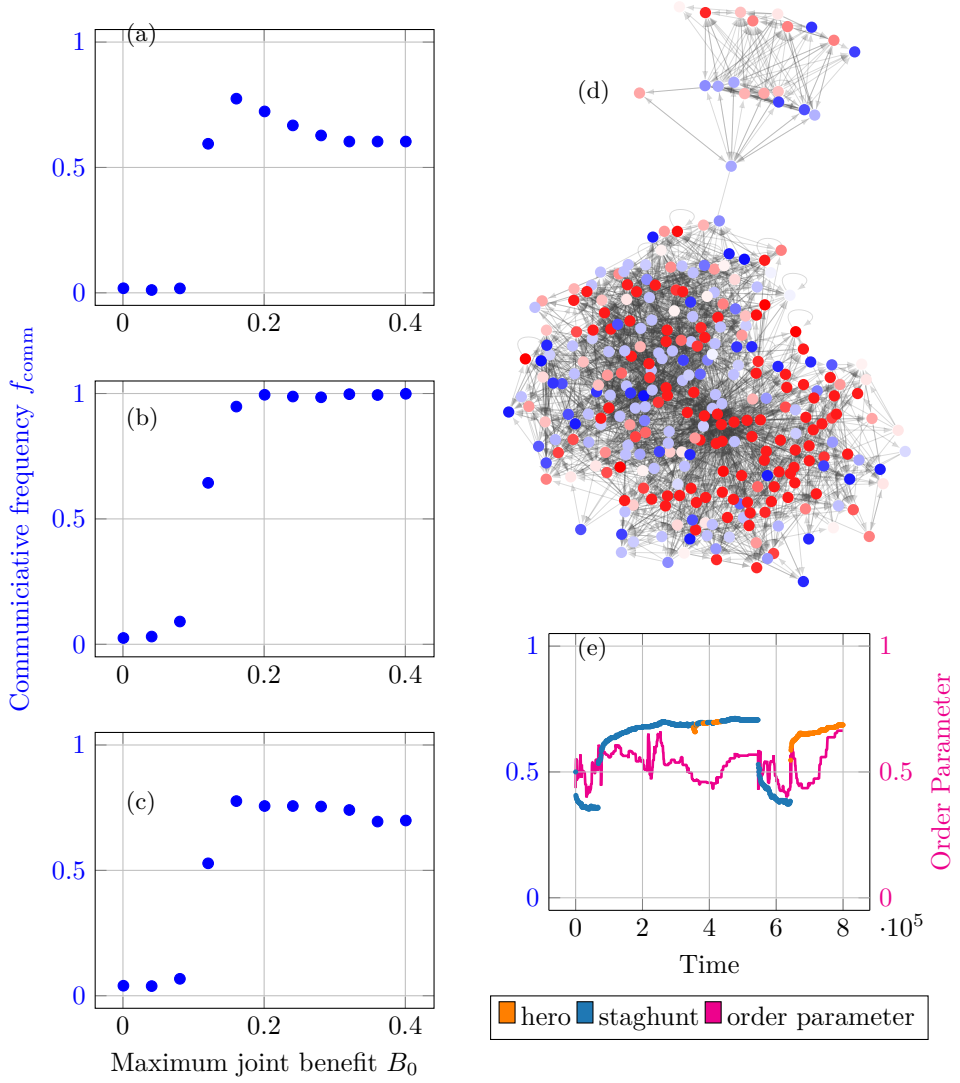


Fig. 4| Rise of chimera states in *C. elegans* neural network. (a)–(c) Time-averaged fraction of players that are communicative as a function of the maximum joint benefit B_0 . The network topologies are the (a) weighted, directed *C. elegans* connectome, (b) unweighted, directed *C. elegans* connectome, and (c) weighted, undirected *C. elegans* connectome. (d) The network topology for the *C. elegans* $N = 300$ weighted, directed connectome with asymmetry $\alpha = 0.75$. The colors represent the $2m = 40$ strategies at a particular time step; blue colors are communicative, red colors are non-communicative, and shades represent different phases ϕ . (e) Scatter plot with the same axes and coloring as Figs. 3(b) to 3(d) showing the communicative frequency, plurality mixed game-types, and order parameter.

from the Fig. 3(a) well-mixed behavior by looking at variations to the Fig. 4(a) *C. elegans* network topology. First, the (b) *directed*, unweighted connectome is qualitatively similar to the (a) well-mixed case with a monotonic increase from low communicativeness for $B_0 < 0.1$ to full communicativeness for $B_0 \geq 0.2$. This implies that directedness plays only a small role in the qualitative shape of the (a) full *C. elegans* case. Conversely, the (c) *weighted*, undirected connectome looks similar to the (a) full *C. elegans* case, displaying the same plateau at $f_{\text{comm}} \approx 0.7$, though the peak around $B_0 = 0.15$ is less pronounced. This similarity implies that the connectome's edge weights cause most of the deviation between the (a) full *C. elegans* case and the Fig. 3(a) well-mixed case.

We can also investigate the time-evolution of the *C. elegans* system using the same parameters as the Figs. 3(b) to 3(d) well-mixed case but with the *C. elegans* connectome graph. Compared to the well-mixed case, the (e) *C. elegans* case depicts a far more heterogeneous population. Here, the population never stabilizes to a fully communicative or non-communicative state. Instead, both its communicative frequency and order parameter stay between 40 % to 70 %. The mean communicative frequency $f_{\text{comm}} \approx 60\%$ is similar to the expected $f_{\text{comm}} \approx 70\%$ from Fig. 4(a) with $B_0 = 0.15$; the discrepancy likely comes from the stochasticity in this small, 8×10^5 time-step subset. And while the Fig. 3(c) well-mixed setup displays hero, staghunt, and concord plurality mixed game-types, the Fig. 4(e) *C. elegans* setup only displays hero and staghunt games. Finally, the *C. elegans* case is less stable to mutations than the Fig. 3(c) well-mixed case: instead of stable synchronized states with transient

impulses, the *C. elegans* case depicts disordered states with discontinuous offsets.

2.5 Chimera-like index

Time-lapse animations of the system's time evolution show a subset of the nodes exhibiting high synchronicity with others remaining disordered: this is characteristic of a chimera state. Animations depicting this phenomena are available as supplementary videos, and an interactive website for exploring the full data set through plots and animations is provided in the “Code availability” section at the end of the paper. In order to quantify this chimera-like effect, we will investigate the chimera-like index χ (Eq. 6) and metastability index λ (Eq. 7). As discussed in Section 4.8, the chimera-like index measures the coherence difference between communities of players, is equal to the time-averaged community covariance, and has a theoretical maximum value of $M/[4(M - 1)] = 0.5$ ²⁰ for our $M = 2$ communities. Conversely, the metastability index represents how often the system transitions between synchronicity and disorder, is equal to the community-average of the temporal covariance, and has a practical maximum of 0.08²⁰. Figure 5 shows the (a) chimera-like index χ and (b) metastability index λ as functions of the asymmetry α . These simulations ran with the same parameters as the Figs. 4(a) to 4(c) *C. elegans* time-series data.

The metastability displayed in Fig. 5 is less than 0.01, much smaller than the practical maximum of 0.08. This implies that the system has low metastability and spends most of its time at a nearly constant synchronicity $\rho_m(t)$. Furthermore, while the metastability is higher (more stability variations) at $\lambda \approx 0.01$ for the $\alpha = 0$ case, the metastability drops precipitously for larger α , always staying below

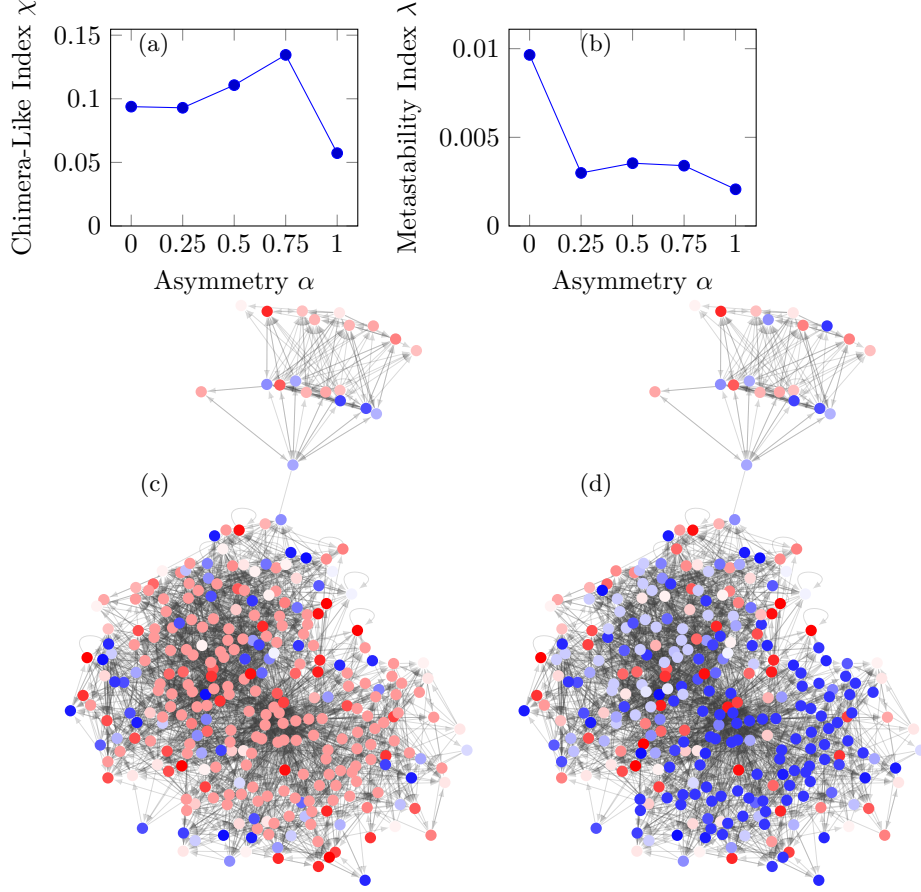


Fig. 5| Characterizing chimera states. (a) The chimera-like index (Eq. 6) and (b) metastability index (Eq. 7) as functions of the asymmetry α for the weighted, directed *C. elegans* connectome. To calculate the indices, we split the graph into two communities according to the nodes' relative covariance (cf., Section 4.8). (c)–(d) A snapshot of the *C. elegans* connectome where blue colors are communicative, red colors are non-communicative, and shades represent different phases ϕ . The asymmetry is (c) $\alpha = 0$ or (d) $\alpha = 1$.

0.004 implying that higher asymmetry α makes the system more stable. Conversely, the chimera-like index χ indicates a high chimeric quality with values (0.06 to 0.13) nearly a quarter of the theoretical maximum (0.5). Given that we average the chimera-like index over time, the system's deviation from a complete chimera state

arises from both imperfect separation of the coherent/disordered populations as well as time fluctuations in the chimeric quality. While we observe that χ has a maximum at $\alpha = 0.75$, we caution that this is likely the result of calculating the communities based on the $\alpha = 0.75$ covariances. Nevertheless, the high χ value for

all asymmetries α implies that the strong chimeric character is intrinsic rather than an artifact of our $\alpha = 0.75$ choice.

2.6 Game types

Next, we seek to understand the types of games that nodes play during the population's evolution. In Fig. 6, we investigate the plurality game type amongst all player interactions at each time step (*cf.*, Section 4.6). Figure 6 shows the fraction of time that a given game type is the plurality for different values of the asymmetry α for (a) $N = 20$ well-mixed, and (b) *C. elegans* connectome network topologies. The (a) well-mixed case fully-synchronized to all-communicative or all-noncommunicative for over 99.6 % of the runtime across every asymmetry α , as corroborated by the order parameter $\rho \approx 1$ in Figs. 3(b) to 3(d). Furthermore, the α -dependence of the communicative synchronization (“all-C”) fraction approximates the communicative frequency f_{comm} in Fig. 3(a) for $B_0 = 0.15$. In contrast, the (b) *C. elegans* system is never synchronized, but instead is virtually always dominated by coordination (CC) and neutral (NN) game types.

In order to investigate the other game types involved, we can also consider the plurality *mixed* game type (*cf.*, Section 4.6). The (c) well-mixed case only changes for the < 1 % of the time when unsynchronized. In order to better observe these games types, a blue inset below Fig. 6(c) magnifies these small fractions. In contrast, the (d) shows a variety of most-frequent game types that vary based on the asymmetry: dilemma for $\alpha = 0, 0.25$, chicken for $\alpha = 0.5$, hero for $\alpha = 0.75$, and deadlock for $\alpha = 1$. We note that these dominant game types are the same as the most-frequent *disordered* (*i.e.*, states other than “all-C” or

“all-N”) plurality mixed games as those played in the Fig. 6(c) well-mixed setup (*cf.*, blue inset) for each α . Additionally, the *C. elegans* system displays some game-type heterogeneity, with a second game type (staghunt) being the plurality 1 % to 18 % of the time for asymmetries $\alpha \geq 0.5$. Overall, we see that graph structure decreases synchronization and asymmetry influences the dominant game types, which, in turn, underpin the formation of chimera states.

3 Discussion

We can validate our Fig. 6(c) well-mixed time-series results by comparing the $\alpha = 0.5$ case to previous studies⁶. Their weak-selection $\delta = 0.2$ results also show the system spending virtually all of its time in a synchronized state. When not synchronized, their system had plurality chicken (denoted “snowdrift” therein) and staghunt (denoted “coordination”, not to be confused with the coordination-type game here) games. Indeed, Fig. 2(a) shows that staghunt, dilemma, and chicken would be the only game types accessible for $\alpha = 0.5$, which is corroborated in our simulations by the inset below Fig. 6(c).

Next, we will discuss the observed chimera states. While the chimera-like quality is inherently time-dependent (*cf.*, Eq. 6) carefully chosen snapshots can still convey some of the chimera-like aspects. Figure 5(c) shows a snapshot of the communication strategies for asymmetry $\alpha = 0$ using the same color scheme as Fig. 4(d). We notice a large region of light red representing a synchronized group of non-communicators, as well as a mix of disordered neighbors. This coexistence of strong synchronization and disorder is consistent with the high chimera-like index χ observed in Fig. 5 for $\alpha = 0$. Likewise, the

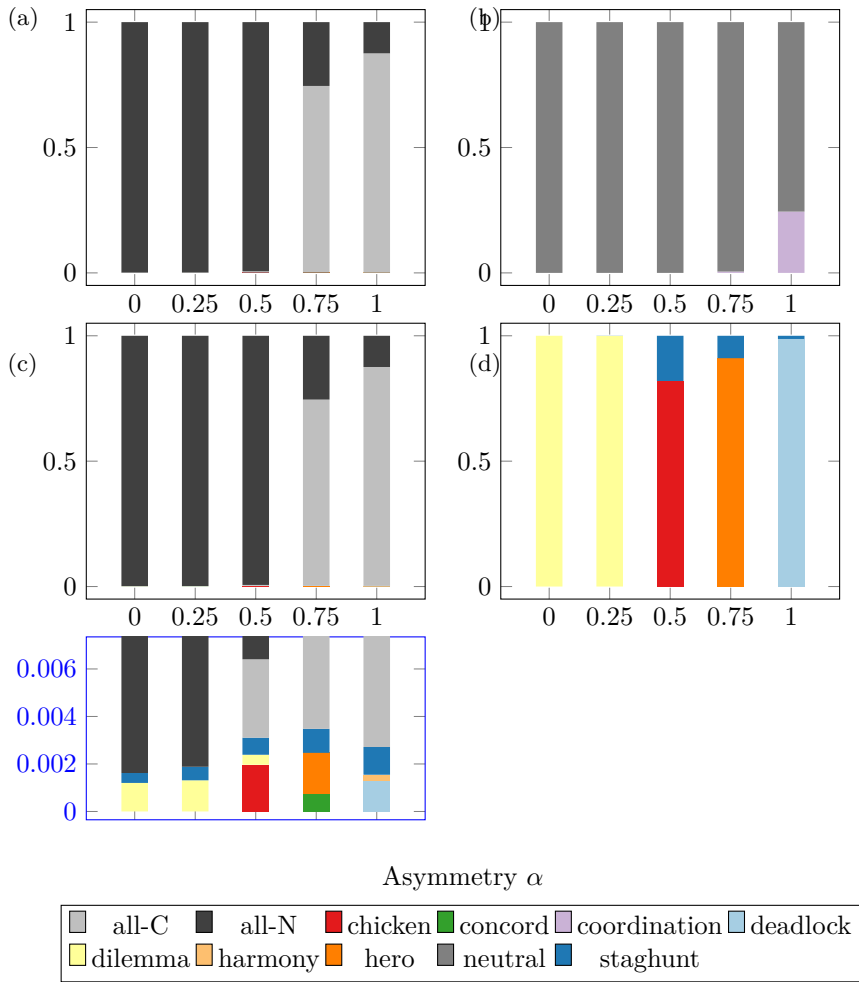


Fig. 6| Influence of payoff asymmetry on game types played. The plurality game type amongst all player interactions expressed as a fraction of all games played for different values of the asymmetry α . The game types are color-coded according to the legend; additionally, “all-C” and “all-N” represent when the population is entirely synchronized to communicativeness or non-communicativeness, respectively. The network topologies are the (a) $N = 20$ well-mixed population and (b) weighted, directed *C. elegans* connectome. Similarly, (c), (d) depict the plurality game type when only considering mixed game types for the (c) $N = 20$ well-mixed population and (d) weighted, directed *C. elegans* connectome. A blue inset below the (c) well-mixed panel shows the magnified lower region.

$\alpha = 0.75$ case depicted in Fig. 4(d) has an even higher $\chi = 0.13$, consistent with the coexistence of a large, synchronized non-communicative group (red) and disordered neighbors (varying phases/colors). In contrast, Fig. 5(d) shows a snapshot for $\alpha = 1$, for which we expect a lower chimera-like index of $\chi = 0.06$. Indeed, we see that the large communicative (red) group in Fig. 5(d) or Fig. 4(d) has fractured into two communicative (blue) groups with different phases (color shade), lowering the chimeric quality. Therefore, these snapshots give a glimpse of the chimera-like quality in the *C. elegans* populations.

We also note that Fig. 6 shows that the high chimera-like index setups ($\alpha = 0.5, 0.75$) are dominated by game types (chicken, hero, and battle), shown in warm colors (red, orange, and pink, respectively), with exponentially slow fixation times²¹. In contrast, the lower chimera-like index setup ($\alpha = 0, 0.25, 1$) is dominated by non-exponentially-slow dilemma and deadlock type games. This connection between exponentially-slow fixation time games and high chimera index seems suggestive and requires further investigation.

Another study of the *C. elegans* connectome also found chimera-like states using an entirely non-game-theory tool, modular neural networks⁴. That study found a maximum chimera-like index of 0.12, in agreement with our value of 0.13, despite the different network models of the *C. elegans* connectome considered. This agreement between two different models of neurons reveals that the emergence of chimera states is most likely primarily driven by the connectivity structure itself.

Chimera states of networked oscillators exhibit coexisting synchronized and disordered populations, are present in brains^{1,2}, and may be pivotal in human

cognition². Prior studies¹⁸ investigated chimera-like brain states in *Drosophila melanogaster* (*D. melanogaster*) using sinusoidally-coupled Kuramoto oscillators, a frequent model for neuron dynamics¹⁷. However, the small-scale evolutionary factors leading to chimera-like states remains poorly understood. In this paper, we extended the evolutionary Kuramoto model to include weighted, structured interaction graphs and an asymmetry between the communicator and non-communicator payoffs. We first applied this model to a well-mixed population and found that increasing (decreasing) the asymmetry inhibits (promotes) communicativity. Next, we applied the model to a family of graphs deriving from the *C. elegans* connectome. This revealed that the graph's weightedness has a much stronger influence on the communication frequency than the graph's directedness does. Finally, while the well-mixed players have homogeneous populations that occasionally switch between synchronized communicative and non-communicative states, the *C. elegans* population remains far more heterogeneous with a stable, chimeric mix of disordered game types.

Future work will focus on applying the EK model to families of generative brain network models²². The limited number of empirical graphs analyzed in this study hinders the identification of exact relationships between the communicative fraction and graph properties such as edge degree, weight, and directionality. However, applying the model to parameterized families of graphs could allow for fine-tuning the parameters to extract these relations. Additionally, since this study only considers a single species' connectome, it is unclear if our findings regarding the dependence of chimeric activity on

graph structure are generalizable. Therefore, it is of interest to investigate this connection further by applying our EK setup to other model organisms, such as that of *Drosophila melanogaster*²³.

A key takeaway from this study was the importance of edge weight on communicativity; this has important parallels to neural computing, where edge weights are a primary driver of functionality. Additionally, the observation of chimeric states arising from such simple neurogame-theoretic models implies that the nature of neuron interactions is likely a key component in producing these critical brain states. Overall, evolutionary graph theory allowed us to connect low-level payoff details for individual neurons to high-level phenomena such as chimera-states, and this model could serve as a valuable computational framework for clarifying the influence of network structure on neural dynamics.

4 Methods

4.1 Game setup

We model the system of evolving, coupled oscillators by discretizing the 2π phase angle into m discrete phases $2\pi j/m$ for $j \in 0, \dots, m-1$. The game's strategy space is the outer product of the m phases ($m = 20$ for our simulations) and 2 communicative choices, communicative C and non-communicative N . For a given pair of phases, ϕ_i and ϕ_j , the game is specified by the payoff matrix. If one player is communicative and the other is non-communicative ("mixed game", CN or

NC), the payoff matrix is

$$\begin{array}{c|c} C, \phi_i & N, \phi_j \\ \hline C, \phi_i & \begin{array}{c|c} B_0 f(0) - c & 2\alpha\beta_0 f(\Delta\phi) - c \\ \hline 2(1-\alpha)\beta_0 f(\Delta\phi) & 0 \end{array} \\ N, \phi_j & \end{array}, \quad (1)$$

if both players are communicative (CC), the matrix is

$$\begin{array}{c|c} C, \phi_i & C, \phi_j \\ \hline C, \phi_i & \begin{array}{c|c} B_0 f(0) - c & B_0 f(\Delta\phi) - c \\ \hline B_0 f(\Delta\phi) - c & B_0 f(0) - c \end{array} \\ C, \phi_j & \end{array}, \quad (2)$$

and if both are non-communicative (NN), the matrix is

$$\begin{array}{c|c} N, \phi_i & N, \phi_j \\ \hline N, \phi_i & \begin{array}{c|c} 0 & 0 \\ \hline 0 & 0 \end{array} \\ N, \phi_j & \end{array}, \quad (3)$$

with $f(\Delta\phi) = [1 + \cos(\phi_j - \phi_i)]/2$ (Fig. 1(c)). Here, B_0 , β_0 , α , and c are fixed parameters defining the game. The cost c represents the penalty paid by communicative players, and B_0 and β_0 are the maximum benefits paid with joint CC communicators and mixed CN players, respectively. The phase-dependent function $f(\Delta\phi)$ encodes the influence of phase mismatches. Finally, the benefit asymmetry $\alpha \in [0, 1]$ breaks the symmetry between the payoff for the communicator and the non-communicator when exactly one player is communicative.

4.2 Population setup

Given N players, we associate a pair of weighted, directed graphs to the population. First, we use an interaction graph with N nodes representing players and weighted, directed edges representing games between players. Second, we implement a reproduction graph with the N nodes still representing players but the

edges now corresponding to the ability of nodes to replace one another. For simplicity, our reproduction graphs are identical to the interaction graph with a single self-loop added to each node. These self-loops are necessary in the reproduction graph to ensure that each node has positive indegree as required by the Moran process described in the next section.

4.3 Birth-death Moran process

The population is updated according to a birth-death Moran process with exponential fitness²⁴. On each turn, the following steps are performed. First, each edge in the interaction graph corresponds to a game between head node i and tail node j , the edge's payoff π_{ji} is scaled by the edge weight w_{ji} , and the relevant payoff $w_{ji}\pi_{ji}$ is awarded to the head node only. Since the *C. elegans* edge weights are integers, we can also interpret each edge weight as the number of games played between the two nodes. Figure 1(b) shows an illustration of this process for a single pair of interacting players connected by a pair of weighted, directed edges. The total fitness for node i is the exponential of the product between the selection strength δ and the sum of payoffs to node i , or $f_i = \exp(\delta \sum_j w_{ji}\pi_{ji})$ with the sum over all edges inwardly incident to node i . Then, a single focal node is chosen for reproduction with probability proportional to the node's fitness f_i . Finally, a node is chosen for replacement amongst the birth node's out-neighbors with probability proportional to the reproduction graph's edge weight. With mutation probability μ , the death node is replaced by a player with a uniformly random strategy; otherwise, it is replaced by a player with the same strategy as the birth node. This

birth-death process is repeated for each turn.

4.4 Communication frequency

We define the frequency of communicative strategies $f_{\text{comm}}(t)$ as the fraction of players employing a communicative strategy C at a given time step. We also define the time-averaged communicative frequency f_{comm} by averaging $f_{\text{comm}}(t)$ over the entire simulation. For simulation times long compared to the mutation turnover time $T_{\text{turn}} \gg N/\mu$, the initial, random distribution of strategies will be negligible and the time-average will correspond to the long-time limit. In section 2 of the supplementary material, we derive an analytic expression (Eq. 10 of supplementary materials) for f_{comm} in the well-mixed case by incorporating the benefit asymmetry α .

4.5 Game type nomenclature

Every edge of the interaction graph defines a game between the two players it connects. Using their relative phase difference $\Delta\phi$, we can calculate the payoff matrix. By comparing the order of each of the four entries, we determine the game type using a topological taxonomy¹⁹. Using this taxonomy, we calculate the ordinal rank of the four entries in the Eq. (1) payoff matrix and assign a unique name (*e.g.*, dilemma, deadlock, chicken, *etc.*) to each strict, symmetric game type. However, Fig. 2(b) shows that some mixed CN games lie on the border between two game types, such as when $\alpha = 1$ or $B/c = 0$ (bordering game types for $B/c > 0$ and $B/c < 0$, not shown). The taxonomy¹⁹ classifies these non-strict games according the number and location of ties (“high tie”, “middle tie”, “double tie”, *etc.*). It also defines a convention for choosing one of

the neighboring game types to get a binomial nomenclature (*e.g.*, “high harmony”, “mid compromise”, “double coordination”, *etc.*). We follow the same convention for choosing a neighboring game but drop the tie-indicator to keep our figure legends simple. Specifically, referring to Fig. 2(b), the $\alpha = 1$ tie between deadlock and compromise games formally corresponds to “low [dead]lock”, but we label it as deadlock; similarly, the tie between assurance and staghunt is “mid staghunt”, but we denote it as staghunt. Likewise, all of the $B/c = 0$ payoff matrices correspond to the “double harmony” game type, but we denote them as simply “harmony”. Finally, the NN game type is always “neutral” while the CC game type is always “double cooperation”, which we denote as just “cooperation”.

4.6 Plurality game type

At each time step, we calculate the game type for each edge of the interaction graph. We determine the game type by creating a two-by-two payoff matrix of possibilities where both players have the hypothetical option of switching to the other player’s strategy/phase pairing. Using the taxonomy discussed in Section 4.5, we then assign a game type to that interaction. We then identify the plurality game type across all player interactions, where each edge’s count is weighted by its edge weight. Then, we calculate the frequency of this “plurality game” across all time steps of a given simulation to determine the distribution of games commonly played. This “plurality game-type” metric, as depicted in Fig. 6(a) and Fig. 6(a), is often dominated by neutral games (between NN players) and coordination games (between CC) players. To isolate the other game types involved, we also defined a “plurality *mixed* game-type” by

only counting games between mixed CN or NC pairs in the plurality (or labelling the time step as “all-communicative”/“all-noncommunicative”, as necessary). This “plurality mixed game-type” shows more variety and is depicted in all of the other figures (Fig. 3, Fig. 4, Fig. 6(c) and Fig. 6(c)). Note that an edge’s game type is dependent on the players’ dynamically-evolving communication strategies (N or C) and relative phase $\Delta\phi$, as well as the fixed game parameters c , B_0 , β_0 , and α . Furthermore, this metric is only sensitive to the plurality game and therefore provides no information on the presence/absence of minority game types.

4.7 Order parameter

Given that the Kuramoto system of coupled oscillators inspired this evolutionary game model, we also define the standard Kuramoto order parameter:

$$\rho = \frac{1}{N} \left| \sum_{j=1}^N e^{i\phi_j} \right| \quad (4)$$

This parameter ranges from zero to one, inclusive, and represents how coherent the population is, with $\rho = 1$ for fully coherent and $\rho = 0$ fully disordered.

4.8 Chimera-like index and metastability index

To compare with a previous analysis⁴ of chimera-like states *C. elegans* models, we define a pair of indices related to chimera-like quality and metastability²⁰. First, we organize the game’s nodes into M disjoint communities. We split the nodes into $M = 2$ communities C_m by taking a subset (the first 8×10^4 steps for computations ease) of the simulation results for the *C. elegans* simulation with asymmetry

$\alpha = 0.75$. We then calculate the covariance matrix $K_{i,j}$ of the strategy indices, ensuring that communicative (C, ϕ_i) and non-communicative (N, ϕ_i) are treated distinctly. Next, we calculate the row-wise covariance-sums $\sum_i K_{i,j}$ and form a community by collecting all nodes j with covariance-sum at least 1,500, *i.e.*, $\sum_i K_{i,j} \geq 1500$. Note that 1,500 is chosen as a high cutoff to ensure we only group nodes with high covariance-sum; for reference, 1,500 is approximately 81% of the maximum covariance-sum. Finally, we place all the remaining nodes in a second community.

With these disjoint communities C_m , we then calculate the time-dependent, community-wise order parameter $\rho_m(t)$ as

$$\rho_m(t) := \frac{1}{N_m} \left| \sum_{j \in C_m} e^{i\phi_j} \right| \quad (5)$$

across members j of community C_m with size N_m . Then, we define a chimera-like index χ

$$\chi = \langle \sigma_{\text{chi}} \rangle_T \quad (6)$$

where

$$\sigma_{\text{chi}} := \frac{1}{M-1} \sum_{m=1}^M \left(\rho_m(t) - \langle \rho_m(t) \rangle_M \right)^2$$

and a metastability index λ

$$\lambda = \langle \sigma_{\text{met}} \rangle_M \quad (7)$$

where

$$\sigma_{\text{met}} := \frac{1}{T-1} \sum_{t=1}^T \left(\rho_m(t) - \langle \rho_m(t) \rangle_T \right)^2$$

across the M communities and T time steps. The chimera-like index measures the difference in coherence between communities: complete homogeneity between

communities (*e.g.*, all fully synchronized *or* fully disordered) corresponds to $\chi = 0$, while having M communities with half fully synchronized ($\rho_m = 1$) and the other half fully disordered ($\rho_m = 0$) for all times yields a maximum $\chi = M/[4(M-1)] = 1/2$ for our $M = 2^{20}$. Likewise, the metastability index λ measures how metastable the system is (*i.e.*, transiting between synchronicity and disorder). A system that is fully synchronized or disordered gives $\lambda = 0$; λ is maximized for a system spending equal times in each state, where the variance of the uniform distribution gives $\lambda = 1/12 \approx 0.08^{20}$.

Supplementary information. Supplementary Figure 1 of two-player game order graphs. Section 1, two-player game order graphs; Section 2, derivation of well-mixed communicative fraction with symmetry breaking. Supplementary videos 1-3, time-evolution of *C. elegans* player strategies using the same color scheme as Fig. 4(d) with $B_0/c = 1.5$, $\beta_0/B_0 = 0.95$, $c = 0.1$, $\mu = 0.0001$, $m = 20$, $\delta = 0.2$, and 8×10^6 time steps; supplementary video 1 shows $\alpha = 0$, supplementary video 2 shows $\alpha = 0.75$, and supplementary video 3 shows $\alpha = 1$.

Declarations. The authors declare no competing interests.

Code availability. An interactive webpage for exploring the data set is available at https://tzdyski.github.io/egt-kuramoto/notebooks/EKT_Plots.html. Additionally, all source code is available via GitHub at <https://github.com/TZdyski/egt-kuramoto/tree/1.0.0>.

Data availability. The processed data for all simulated parameter ranges is available on Zenodo at <https://doi.org/10.5281/zenodo.17135745>.

References

- [1] Santos, M. *et al.* Chimera-like states in a neuronal network model of the cat brain. *Chaos, Solitons & Fractals* **101**, 86–91 (2017).
- [2] Bansal, K. *et al.* Cognitive chimera states in human brain networks. *Science advances* **5**, eaau8535 (2019).
- [3] Majhi, S., Bera, B. K., Ghosh, D. & Perc, M. Chimera states in neuronal networks: A review. *Physics of life reviews* **28**, 100–121 (2019).
- [4] Hizanidis, J., Kouvaris, N. E., Zamora-López, G., Díaz-Guilera, A. & Antonopoulos, C. G. Chimera-like states in modular neural networks. *Scientific reports* **6**, 19845 (2016).
- [5] Abrams, D. M. & Strogatz, S. H. Chimera states for coupled oscillators. *Physical review letters* **93**, 174102 (2004).
- [6] Tripp, E. A., Fu, F. & Pauls, S. D. Evolutionary kuramoto dynamics. *Proceedings of the Royal Society B* **289**, 20220999 (2022).
- [7] Cook, S. J. *et al.* Whole-animal connectomes of both *caenorhabditis elegans* sexes. *Nature* **571**, 63–71 (2019).
- [8] Towlson, E. K., Vértes, P. E., Ahnert, S. E., Schafer, W. R. & Bullmore, E. T. The rich club of the *c. elegans* neuronal connectome. *Journal of Neuroscience* **33**, 6380–6387 (2013).
- [9] Yan, G. *et al.* Network control principles predict neuron function in the *caenorhabditis elegans* connectome. *Nature* **550**, 519–523 (2017).
- [10] Sigmund, K. & Nowak, M. A. Evolutionary game theory. *Current Biology* **9**, R503–R505 (1999).
- [11] Traulsen, A. & Glynatsi, N. E. The future of theoretical evolutionary game theory. *Philosophical Transactions of the Royal Society B* **378**, 20210508 (2023).
- [12] Cohen, Y. & Cohen, J. Evolutionary game theory and the evolution of neuron populations, ring rates, and decisionmaking. *Nature Precedings* 1–1 (2009).
- [13] Antonioni, A. & Cardillo, A. Coevolution of synchronization and cooperation in costly networked interactions. *Physical review letters* **118**, 238301 (2017).
- [14] Ohtsuki, H., Hauert, C., Lieberman, E. & Nowak, M. A. A simple rule for the evolution of cooperation on graphs and social networks. *Nature* **441**, 502–505 (2006).
- [15] Su, Q., Allen, B. & Plotkin, J. B. Evolution of cooperation with asymmetric social interactions. *Proceedings of the National Academy of Sciences* **119**, e2113468118 (2022).
- [16] Bhaumik, J. & Masuda, N. Constant-selection evolutionary dynamics on weighted networks. *Proceedings of the Royal Society A* **480**, 20240223 (2024).
- [17] Cabral, J., Hugues, E., Sporns, O. & Deco, G. Role of local network oscillations in resting-state functional connectivity. *Neuroimage* **57**, 130–139 (2011).

- [18] Deng, S. & Ódor, G. Chimera-like states in neural networks and power systems. *Chaos: An Interdisciplinary Journal of Nonlinear Science* **34** (2024).
- [19] Bruns, B. R. Names for games: locating 2×2 games. *Games* **6**, 495–520 (2015).
- [20] Shanahan, M. Metastable chimera states in community-structured oscillator networks. *Chaos: An Interdisciplinary Journal of Nonlinear Science* **20** (2010).
- [21] Antal, T. & Scheuring, I. Fixation of strategies for an evolutionary game in finite populations. *Bulletin of mathematical biology* **68**, 1923–1944 (2006).
- [22] Betzel, R. F. *et al.* Generative models of the human connectome. *Neuroimage* **124**, 1054–1064 (2016).
- [23] Schlegel, P. *et al.* Whole-brain annotation and multi-connectome cell typing of drosophila. *Nature* **634**, 139–152 (2024).
- [24] Lieberman, E., Hauert, C. & Nowak, M. A. Evolutionary dynamics on graphs. *Nature* **433**, 312–316 (2005).

Supplementary Information for
“Evolutionary Kuramoto dynamics unravels origins
of chimera states in neural populations”

Thomas Zdyrski, Scott Pauls, Feng Fu

Contents

1	Two-player game order graphs	2
2	Well-mixed communicative fraction with symmetry breaking	3
3	Data availability	8
3.1	Time-evolution animations	8
3.2	Interactive plots	8

1 Two-player game order graphs

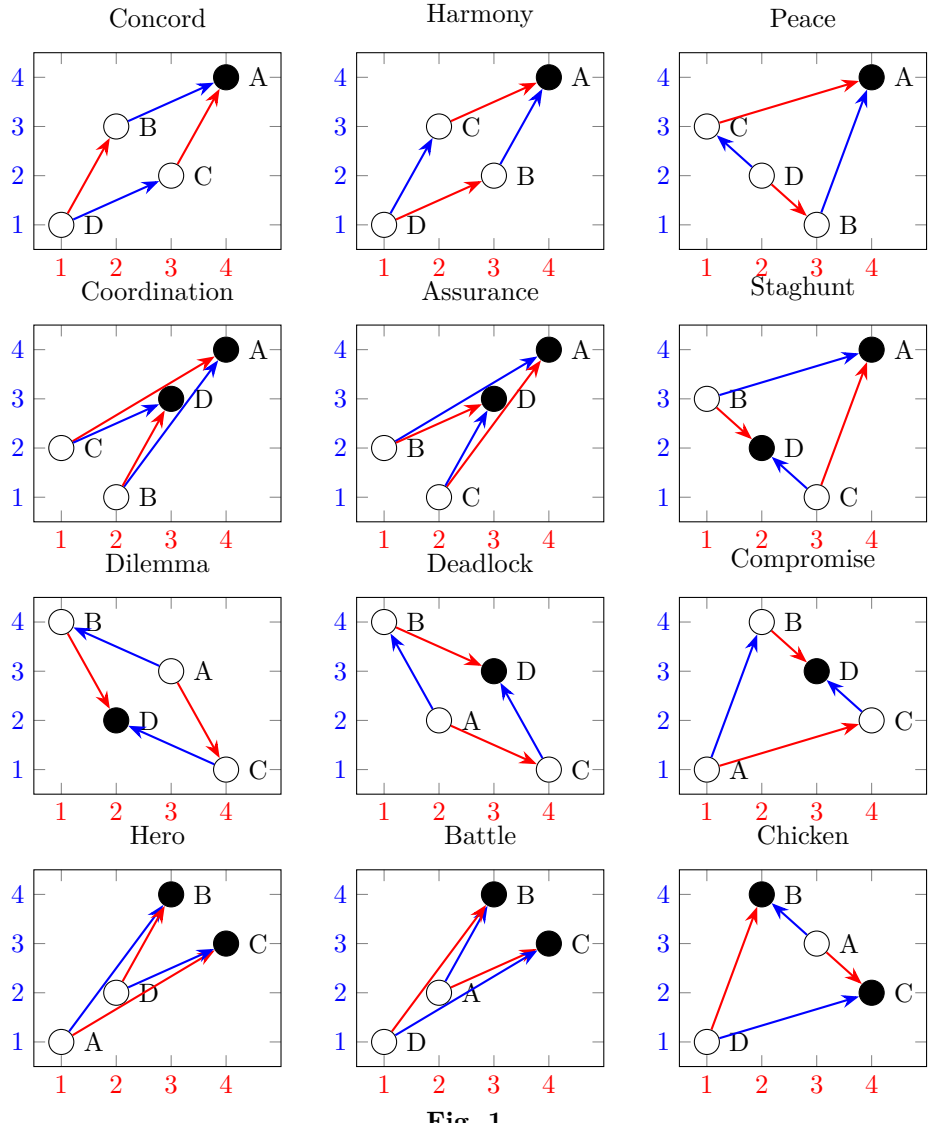


Fig. 1

Figure 1 shows the order graphs for the 16 symmetric, ordinal two-player games. Each sub-panel shows the payoff order for both the column and row player. The letters correspond to the following payoff matrix

$$\begin{array}{c}
 C \ N \\
 \hline
 C \left[\begin{array}{c|c} A & B \\ \hline C & D \end{array} \right] \\
 \hline
 N
 \end{array}$$

The horizontal axis represents the order of row player payoffs, and the red lines represent row player options. The vertical axis represents the order of column player payoffs, and the blue lines represent column player options. The arrows show the direction of increasing payoff for the relevant player, and solid black dots represent Nash equilibria. This figure is adapted from the topological taxonomy order graphs¹.

2 Well-mixed communicative fraction with symmetry breaking

Here, we follow the steady-state communicative fraction derivation in the previous EK study² and extend it to include a payoff asymmetry α . To keep the derivation tractable, we only consider the well-mixed case. We will assume a low mutation rate so that any mutation fixates prior to the next mutation. We then consider a population with one communicative species $E = (C, \phi_i)$ and one non-communicative species $F = (N, \phi_j)$. Our first goal is to calculate the (communicative) ρ_E and (non-communicative) ρ_F fixation probabilities of a single E or F invader, respectively. First, we use our α -dependent payoff matrix, to calculate the α -dependent average payoff of each strategy across the entire population,

$$\pi_E(k) = \left(\frac{k-1}{n-1} \right) (B_0 - c) + \left(\frac{n-k}{n-1} \right) (\beta(\Delta\phi)2\alpha - c) \quad (1)$$

$$= \frac{1}{n-1} \left(k(B_0 - 2\alpha\beta(\Delta\phi)) + 2\alpha n \beta(\Delta\phi) - B_0 - (n-1)c \right) \quad (2)$$

and

$$\pi_F(k) = \left(\frac{k}{n-1} \right) (\beta(\Delta\phi)2(1-\alpha)) + \left(\frac{n-k-1}{n-1} \right) (0) \quad (3)$$

$$= \left(\frac{k}{n-1} \right) 2(1-\alpha)\beta(\Delta\phi) \quad (4)$$

Here, $k \in [0, n]$ is the number of E -players $\Delta\phi$ is the phase difference between the E and F strategies, and we defined $\beta(\Delta\phi) = \beta_0 f(\Delta\phi)$. Note that the first term of π_E corresponds to the E - E payoff, which has $\Delta\phi = 0$, hence $B_0 f(\Delta\phi) = B_0$. As mentioned in the main text, each node has an exponential total fitness $f_E = \exp(\delta(n-1)\pi_E)$ or $f_F = \exp(\delta(n-1)\pi_F)$, depending on its strategy, with selection strength δ .

In this paragraph, we summarize the relevant steps; see the prior work² for more detailed derivations. We now model the Moran process as a Markov chain where each state $i \in \{0, 1, \dots, n\}$ is the number of (communicative) E strategies. Interestingly, we note that since the Moran process changes, at most, one strategy per time step, this Markov chain has the same fixation probabilities as a (state-dependent) “gambler’s ruin” problem with ties. We denote x_i as the probability that state i will fixate to state n with all players using strategy E . Then, the E and F fixation probabilities

defined above are given by $\rho_E = x_1$ and $\rho_F = 1 - x_{n-1}$. Now, the Markov chain is described by the transition probability $p_{i,j}$ from state i to state j as

$$\begin{aligned} p_{0,0} &= 1, \\ p_{n,n} &= 1, \\ p_{i,i-1} &= \frac{i}{n} \frac{(n-i)f_F(i)}{if_E(i) + (n-i)f_F(i)} \\ p_{i,i+1} &= \frac{n-i}{n} \frac{if_E(i)}{if_E(i) + (n-i)f_F(i)} \\ p_{i,i} &= 1 - p_{i,i+1} - p_{i,i-1} \end{aligned}$$

Then, we obtain a recurrence relation for x_i by conditioning on the outcome of the first step:

$$x_i = x_{i-1}p_{i,i-1} + x_ip_{i,i} + x_{i+1}p_{i,i+1}$$

with boundary values

$$\begin{aligned} x_0 &= 0 \\ x_1 &= 1 \end{aligned}$$

Using the $p_{i,i} = 1 - p_{i,i+1} - p_{i,i-1}$ relation from above to replace the $p_{i,i}$ term gives

$$(x_i - x_{i-1})\gamma_i = (x_{i+1} - x_i)$$

Then, defining $y_i := x_i - x_{i-1}$, we find $y_1 = x_1$ and $y_{i+1} = \gamma_i y_i$, yielding $y_i = \prod_{j=1}^{i-1} \gamma_j x_1$ for $i \geq 2$. Finally, we form a telescoping sum to yield

$$1 - x_1 = x_n - x_1 = \sum_{i=1}^{n-1} y_{i+1} = \sum_{i=1}^{n-1} \prod_{j=1}^i \gamma_j x_1$$

Solving this for x_1 gives

$$\rho_E = x_1 = \frac{1}{1 + \sum_{i=1}^{n-1} \prod_{j=1}^i \gamma_j} \quad (5)$$

Likewise, $x_i = \sum_{j=1}^i y_j = \sum_{j=0}^{i-1} y_{i+1}$, so

$$x_i = x_1 + \sum_{j=1}^{i-1} \prod_{k=1}^j \gamma_k x_1 = \frac{1 + \sum_{j=1}^{i-1} \prod_{k=1}^j \gamma_k}{1 + \sum_{j=1}^{n-1} \prod_{k=1}^j \gamma_k}$$

Therefore, we find

$$\rho_F = 1 - x_{n-1} = 1 - \frac{1 + \sum_{j=1}^{n-2} \prod_{k=1}^j \gamma_k}{1 + \sum_{j=1}^{n-1} \prod_{k=1}^j \gamma_k} = \frac{\prod_{k=1}^{n-1} \gamma_k}{1 + \sum_{j=1}^{n-1} \prod_{k=1}^j \gamma_k}$$

This implies

$$\frac{\rho_F}{\rho_E} = \prod_{k=1}^{n-1} \gamma_k \quad (6)$$

Therefore, we've found ρ_E and ρ_F for a population with two fixed strategies.

Now, we need to derive the form of the γ_k , which will include the new asymmetry factor α :

$$\begin{aligned} \gamma_k &= \frac{f_F(k)}{f_E(k)} \\ &= \exp[\delta(n-1)(\pi_F(k) - \pi_E(k))] \\ &= \exp\left[\delta\left(k2(1-\alpha)\beta(\Delta\phi) - k\left(B_0 - 2\alpha\beta(\Delta\phi)\right) - 2\alpha n\beta(\Delta\phi) + B_0 + (n-1)c\right)\right] \\ &= \exp\left[\delta\left(\left(2\beta(\Delta\phi) - B_0\right)k + B_0 - 2\alpha n\beta(\Delta\phi) + (n-1)c\right)\right] \end{aligned}$$

We also calculate

$$\begin{aligned} \prod_{k=1}^j \gamma_k &= \prod_{k=1}^j \exp\left[\delta\left(\left(2\beta(\Delta\phi_{qr}) - B_0\right)k + B_0 - 2\alpha n\beta(\Delta\phi_{qr}) + (n-1)c\right)\right] \\ &= \exp\left[\delta \sum_{k=1}^j \left(\left(2\beta(\Delta\phi_{qr}) - B_0\right)k + B_0 - 2\alpha n\beta(\Delta\phi_{qr}) + (n-1)c\right)\right] \\ &= \exp\left[\delta\left(\left(2\beta(\Delta\phi_{qr}) - B_0\right)\frac{j(j+1)}{2} + j\left(B_0 - 2\alpha n\beta(\Delta\phi_{qr}) + (n-1)c\right)\right)\right] \\ &= \exp\left[\delta\left(\left(\beta(\Delta\phi_{qr}) - \frac{B_0}{2}\right)j^2 + j\left(\frac{B_0}{2} + \beta(\Delta\phi_{qr})(1 - 2\alpha n) + (n-1)c\right)\right)\right] \end{aligned} \quad (7)$$

Additionally, we note that substituting Eq. (7) into Eq. (6) with $j = n-1$ shows that ρ_F/ρ_E depends of $\Delta\phi_{qr}$. This is in contrast to the $\alpha = 0.5$ case² where ρ_F/ρ_E simplifies to the $\Delta\phi_{qr}$ -independent form $\rho_F/\rho_E = \exp\left(\delta\left[(n-1)c - B_0(n-2)/2\right]\right)$.

Next, we consider the long-time dynamics incorporating more than two strategies. By again using the low-mutation-rate assumption, we can assume that any mutation either fixates or dies out before the next mutation. Therefore, the system

evolves from one homogeneous state to another using the probabilities we just derived. We can model this behavior with a new Markov chain using the $m = 20$ phases and two communicative strategies (C and N) to give a $2m$ -dimensional state space: $\{(C, \phi_1), \dots, (C, \phi_m), (N, \phi_1), \dots, (N, \phi_m)\}$. Then, the transition probability $\rho_{NC, \Delta\phi_{qr}}$ from state (N, ϕ_q) to state (C, ϕ_r) is just ρ_E above. Similarly, the probability $\rho_{CN, \Delta\phi_{qr}}$ that a (C, ϕ_r) state is successfully invaded by an (N, ϕ_q) state is simply ρ_F above. By the rotation symmetry of ϕ , each ϕ_i has the same probability of fixation. Therefore, consider an arbitrary ϕ_q and denote its communicative fixation probability as s_1 and its non-communicative fixation probability s_2 . We can calculate the ratio of these probabilities by incorporating the fixation probabilities against all other ϕ_r phases:

$$\frac{s_2}{s_1} = \frac{\sum_{r=1}^m \rho_{CN, \Delta\phi_{qr}}}{\sum_{r=1}^m \rho_{NC, \Delta\phi_{qr}}} \quad (8)$$

$$= \frac{\sum_{r=1}^m \rho_{NC, \Delta\phi_{qr}} \exp\left\{\delta(n-1)\left[(n-1)c + n\beta(\Delta\phi_{qr})(1-2\alpha) - \frac{n-2}{2}B_0\right]\right\}}{\sum_{r=1}^m \rho_{NC, \Delta\phi_{qr}}} \quad (9)$$

$$= \left[\frac{\sum_{r=1}^m \frac{\exp\left\{\delta(n-1)\left[(n-1)c + n\beta(\Delta\phi_{qr})(1-2\alpha) - \frac{n-2}{2}B_0\right]\right\}}{1 + \sum_{j=1}^{n-1} \exp\left\{\delta\left[\left(\beta(\Delta\phi_{qr}) - B_0/2\right)j^2 + j\left(B_0/2 + \beta(\Delta\phi_{qr})(1-2\alpha)n + (n-1)c\right)\right]\right\}}}{\sum_{r=1}^m \frac{1}{1 + \sum_{j=1}^{n-1} \exp\left\{\delta\left[\left(\beta(\Delta\phi_{qr}) - B_0/2\right)j^2 + j\left(B_0/2 + \beta(\Delta\phi_{qr})(1-2\alpha)n + (n-1)c\right)\right]\right\}}} \right] \quad (10)$$

The first equality used Eq. (6) and the second equality used Eq. (5). Unlike in the $\alpha = 0.5$ symmetric case², the ratio ρ_F/ρ_E depends on $\Delta\phi_{qr}$, so we cannot factor the exponential component out of the sum and cancel the $\rho_{CN, \Delta\phi_{qr}}$ terms. However, we can asymptotically expand s_2/s_1 for small $B_0/c := \epsilon \ll 1$; additionally, since all of our simulations use $\beta \propto B$, we also assume $\beta/c \sim \epsilon \ll 1$. Finally, to simplify the calculation, we define the asymptotic expansion of $\rho_{NC, \Delta\phi_{qr}} := \rho_{NC, \Delta\phi_{qr}}^{(0)} + \rho_{NC, \Delta\phi_{qr}}^{(1)} + \mathcal{O}(\epsilon^2)$ where $\rho_{NC, \Delta\phi_{qr}}^{(i)} \sim \epsilon^i$ depends only on terms of total order i in B_0/c and β/c .

Then, to first order in ϵ we have

$$\begin{aligned} \frac{s_2}{s_1} &= \frac{\sum_{r=1}^m \rho_{NC, \Delta\phi_{qr}} \exp\left\{\delta(n-1)\left[(n-1)c + n\beta(\Delta\phi_{qr})(1-2\alpha) - \frac{n-2}{2}B_0\right]\right\}}{\sum_{r=1}^m \rho_{NC, \Delta\phi_{qr}}} \\ &= e^{\delta(n-1)^2 c} \left\{ \dots \right\} \end{aligned}$$

$$\begin{aligned}
& \frac{\sum_{r=1}^m \left(\rho_{NC, \Delta\phi_{qr}}^{(0)} + \rho_{NC, \Delta\phi_{qr}}^{(1)} \right) \left\{ 1 + \delta(n-1) \left[n\beta(\Delta\phi_{qr})(1-2\alpha) - \frac{n-2}{2}B_0 \right] \right\}}{\sum_{r=1}^m \left(\rho_{NC, \Delta\phi_{qr}}^{(0)} + \rho_{NC, \Delta\phi_{qr}}^{(1)} \right)} \\
& + \mathcal{O}(\epsilon^2) \\
& = e^{\delta(n-1)^2 c} \left\{ \frac{\sum_{r=1}^m \left(\rho_{NC, \Delta\phi_{qr}}^{(0)} + \rho_{NC, \Delta\phi_{qr}}^{(1)} \right)}{\sum_{r=1}^m \left(\rho_{NC, \Delta\phi_{qr}}^{(0)} + \rho_{NC, \Delta\phi_{qr}}^{(1)} \right)} \right. \\
& \quad \left. + \frac{\sum_{r=1}^m \rho_{NC, \Delta\phi_{qr}}^{(0)} \delta(n-1) \left[n\beta(\Delta\phi_{qr})(1-2\alpha) - \frac{n-2}{2}B_0 \right]}{\sum_{r=1}^m \rho_{NC, \Delta\phi_{qr}}^{(0)}} \right\} + \mathcal{O}(\epsilon^2) \\
& = e^{\delta(n-1)^2 c} \left\{ 1 - \delta(n-1) \frac{n-2}{2} B_0 + \frac{\delta n(n-1)}{m} (1-2\alpha) \sum_{r=1}^m \beta(\Delta\phi_{qr}) \right\} + \mathcal{O}(\epsilon^2) \\
& = \exp \left\{ \delta(n-1) \left[(n-1)c - \frac{n-2}{2}B_0 + \frac{n(1-2\alpha)}{m} \sum_{r=1}^m \beta(\Delta\phi_{qr}) \right] \right\} + \mathcal{O}(\epsilon^2) \\
& = \exp \left\{ \delta(n-1) \left[(n-1)c - \frac{n-2}{2}B_0 + \frac{n(1-2\alpha)}{2} \beta_0 \right] \right\} + \mathcal{O}(\epsilon^2)
\end{aligned}$$

Where, in the last line, we used the definition of $\beta(\Delta\phi_{qr}) = \beta_0 [1 + \cos(\Delta\phi_{qr})]/2$ to write $\sum_{r=1}^m \beta(\Delta\phi_{qr}) = \beta_0 \sum_{r=1}^m \left\{ 1 + \cos[2\pi(q-r)/m] \right\}/2 = m\beta_0/2$ since the cosine sum gives zero.

Finally, since each $\Delta\phi_i$ is equally likely, the probability of fixing to *any* communicative state is ms_1 ; likewise the total non-communicative fixation probability is ms_2 . Then, since the process must eventually absorb to either C or N , we have $ms_1 + ms_2 = 1$, giving the probability of communicative fixation as

$$ms_1 = \frac{1}{1 + s_2/s_1} \tag{11}$$

with s_2/s_1 given by Eq. (10), and the asymptotic, small- ϵ approximation given by

$$ms_1 = \frac{1}{1 + s_2/s_1} \approx \frac{1}{1 + \exp \left\{ \delta(n-1) \left[(n-1)c - \frac{n-2}{2}B_0 + \frac{n(1-2\alpha)}{2} \beta_0 \right] \right\}} \tag{12}$$

3 Data availability

3.1 Time-evolution animations

The chimera-like quality of the games' populations are necessarily time-dependent. We found that animations showing the time-evolution of players' strategies was a particularly useful way to observe this chimera-like quality. Therefore, we have included animations showing the populations' evolving strategies in the supplemental information for a subset of the parameters sampled.

3.2 Interactive plots

While discussing the simulation results in the main manuscript, we necessarily focused on a particular region of parameter space. Nevertheless, we also performed simulations across a range of parameters to ensure the robustness of our results. We used a Pluto.jl notebook to organize and visualize the data and have made these results available for public analysis. Additionally, this notebook includes time-evolution animations for all of the simulated parameter combinations.

References

- [1] Bruns, B. R. Names for games: locating 2×2 games. *Games* **6**, 495–520 (2015).
- [2] Tripp, E. A., Fu, F. & Pauls, S. D. Evolutionary kuramoto dynamics. *Proceedings of the Royal Society B* **289**, 20220999 (2022).